JOURNAL OF CATALYSIS **179,** 537–547 (1998)
ARTICLE NO. CA982249

Mild Hydrocracking of Vacuum Gasoil over NiMo-Beta Zeolite Catalysts: The Role of the Location of the NiMo Phases and the Crystallite Size of the Zeolite

M. A. Camblor,* A. Corma,* A. Martínez,*,[1] V. Martínez-Soria,† and S. Valencia*

*Instituto de Tecnología Química, UPV-CSIC, Avenida de los Naranjos s/n. 46022, Valencia, Spain; †Departamento de Ingeniería Química, Universitat de València, 46100, Burjassot, Spain

Received May 13, 1998; revised August 5, 1998; accepted August 5, 1998

Mild hydrocracking composite catalysts based on NiMo/γ-Al_2O_3-Beta zeolite have been prepared and the influence of the location of the NiMo phases has been studied. A good hydrocracking activity and the highest HDS conversion was found during the hydrocracking of a vacuum gasoil with the composite catalyst where the NiMo is located on the alumina component and then mixed with the zeolite in a proportion of 1 : 1 by weight. The crystal size of the beta zeolite had a significative influence on the catalytic behaviour, being better the smaller the crystallite size is. The small crystallite beta-based catalyst displayed a higher hydrocracking activity than conventional USY and silica-alumina-based catalysts, giving a good selectivity towards middle distillates. © 1998 Academic Press

Key Words: **mild hydrocracking; zeolite; NiMo, beta; crystallite size.**

1. INTRODUCTION

In the last years the demand for high quality diesel fuels has experienced a spectacular increase that is expected to continue in the near future. Taking this into account, it is not surprising that hydrocracking processes will play an important role in the modern refinery schemes (1), and consequently the significant increase in the hydrocracking capacity projected (2). One of the most important characteristics of hydrocracking is its flexibility to convert a wide range of feedstocks to a variety of products. When the process is maximized for middle distillate production, an excellent diesel fuel blendstock having high cetane number and very low sulfur content is obtained.

In addition to conventional hydrocracking, refiners have turned their interest towards mild hydrocracking (MHC) processes (3). Catalysts used for MHC are similar to those used for hydrotreating but the support has to be mildly acidic in order to crack the feed molecules. Typical supports for MHC are amorphous silica-alumina, a zeolite with reduced acidity, such as a low unit cell size USY zeolite, and fluorine-doped alumina (3, 4). MHC usually produces high yields of low-sulfur fuel oil, which can be an excellent feedstock for catalytic cracking (FCC) units, and lower yields of middle distillates of a medium quality (5). Then, it is highly desirable to develop new hydrocracking and MHC catalysts that can maximize the production of middle distillates while keeping, or even increasing, the quality of the final product. For this purpose, zeolites offer advantages over amorphous silica-alumina since they can operate at lower reaction temperatures, thus favoring the hydrogenation of the aromatics present in the feed and increasing the cetane number of the diesel produced (6). Furthermore, and if the production of middle distillates has to be maximized, one should avoid as much as possible the recracking of the molecules formed in the primary cracking events when diffusing out of the zeolites pores. These problems can be attacked, on one hand, by producing crystalline molecular sieves with improved accessibility to the acid sites. In this line of work, MCM-41 based hydrocracking catalysts have shown (7) an improved activity and selectivity for fuel production, at least when they are calculated per unit weight of catalyst. In the case of microporous materials, the most successful solution relies on increasing the mesoporosity in the crystals by postsynthesis treatments or by using zeolites with smaller crystallites (8).

In this sense, faujasite Y zeolite has been synthesized with small crystallites, but unfortunately its hydrothermal stability is not high enough and a considerable loss of crystallinity is produced during the activation–dealumination process (8), unless the Y zeolite is synthesized with a higher Si/Al ratio (9). This is still an active research field which is so far limited by the cost of the final material.

The large pore Beta zeolite has also shown its ability as a component of hydrocracking catalysts (10, 11), but the cost of the zeolite together with the high selectivity to gases has been limiting the commercial application. It is then of

[1] To whom correspondence should be addressed. E-mail: amart@itq.upv.es.

0021-9517/98 $25.00
Copyright © 1998 by Academic Press
All rights of reproduction in any form reserved.

interest to increase the activity and to improve the selectivity of hydrocracking catalysts based on beta zeolite. We thought that this could be done by using beta zeolite with very small crystallites. In this case, while increasing the external surface the length of the pores will be reduced and therefore will increase activity and selectivity to middle distillates. In the case of beta zeolite, by being a high Si/Al ratio zeolite, is hydrothermally more stable and therefore it does not require severe activation treatments.

In this work we have studied the catalytic performance of NiMo-catalysts based on beta zeolite for the mild hydrocracking of a vacuum gasoil (VGO) at mild pressures (3.0–5.0 MPa), and temperatures in the range of 375–425°C. The influence of the acid site density and crystal size has also been studied by preparing two nanocrystalline beta samples (12) with different Si/Al ratio (8 and 17) and by comparing the results with a beta sample synthesized within large crystals. The importance of the location of the metal sulfides in the final zeolite-based catalysts is presented, and finally, the activity and selectivity of the NiMo-catalysts based on nanocrystalline beta zeolite are compared with those obtained using amorphous silica-alumina and USY zeolite.

1. EXPERIMENTAL

1.1. Synthesis of Zeolites and Preparation of the Final NiMo-Catalysts

Synthesis of Nanocrystalline Beta Samples

Two nanocrystalline beta samples differing in their Si/Al atomic ratio were synthesized without alkali cations and seeding (12). For these syntheses a solution of metal aluminum (Merck, 99.95%) in tetraethylammonium hydroxide (TEAOH, Aldrich, 35% aqueous solution, Na < 2 ppm, K < 0.5 ppm) was added to a homogeneous solution of silica (Aerosil 200, Degussa) dispersed in TEAOH, and the mixture was homogenized by stirring. The molar composition of the gels can be expressed as:

Sample NB8: $Al_2O_3 : 16\ SiO_2 : 10.3\ TEAOH : 240\ H_2O$;

Sample NB17: $Al_2O_3 : 50\ SiO_2 : 28.0\ TEAOH : 750\ H_2O$.

Crystallization was carried out in teflon-lined stainless steel autoclaves (60 ml) at 140°C under rotation (60 rpm) during about 30 and 5 days for sample NB8 and NB17, respectively. Then, the solids were separated by centrifugal filtration at 16,000 rpm for 90 min, washed with distilled water until the pH was lower than 9, and dried at 100°C. Finally, the samples were thermally treated at 540°C during 1 h in nitrogen flow and then 6 h in air flow. The Si/Al atomic ratio of the calcined solids was 8 and 17 for samples NB8 and NB17, respectively, as determined by chemical analysis.

Synthesis of Zeolite Beta in Fluoride Medium

For comparison purposes, a sample of beta zeolite (BF9) has been synthesized in the presence of fluoride anions at near neutral pH (below 9.5) following the procedure described in Ref. (13). This method of synthesis produces beta samples with a lower concentration of structural defects and with much larger crystals, as compared to the conventional methods of synthesis in basic medium (13). The molar composition of the gel prepared for the synthesis of sample BF9 was

$$Al_2O_3 : 16\ SiO_2 : 9.7\ TEAOH : 126\ H_2O : 9.7\ HF.$$

The gel was crystallized in 60 ml PTFE lined stainless steel autoclaves at 140°C under rotation (60 rpm) during 6.5 days. The solid was filtered, washed with distilled water, and dried at 100°C. Then, the final zeolite was converted into the protonic form by calcination using the same protocol as for the nanocrystalline samples. The Si/Al atomic ratio of the calcined solid was found to be 9 from chemical analyses.

Commercial Supports

A commercial beta zeolite (CP811 from PQ Corp., Si/Al ratio of 12, protonic form, referred to as BPQ) was used in this work in order to study the influence of the location of the NiMo phase in the final performance of the composite hydrocracking catalyst (see below).

A commercial USY zeolite (CBV500, PQ Corp.), an amorphous silica-alumina (25% Al_2O_3, Crossfield), and γ-Al_2O_3 (Merck) were also used as reference supports.

Impregnation of NiMo

NiMo catalysts were prepared by sequential incipient wetness impregnation, with Mo being impregnated first. Thus, the required amount of an aqueous solution of ammonium heptamolybdate was impregnated on the support, followed by calcination at 500°C for 3 h in air, using a temperature ramp of about 2°C/min. Then, an aqueous solution of nickel nitrate was impregnated and the samples were finally calcined at 500°C for 3 h as above.

For the study of the influence of the location of the metal sulfides on the hydrocracking activity the metals precursors (15 wt% MoO_3 and 4 wt% NiO) were impregnated either on the zeolite alone (NiMo/BPQ), on a mechanical mixture of the zeolite and γ-alumina (NiMo/(Al + BPQ)), or on a separate γ-Al_2O_3 component (NiMo/Al), and then mixed with the acidic zeolite in a 1:1 or 1:2 NiMo/Al to zeolite ratio (wt/wt) to produce sample ((NiMo/Al) + BPQ). In this case two catalysts were prepared by physically mixing the NiMo/Al and the zeolite in a 1:1 or 1:2 wt/wt ratio, then the mixture is molturated, pressed, and sieved to the desired particle size. The composition of the catalysts prepared for this part is shown in Table 1.

TABLE 1

Composition and Physicochemical Properties of the NiMo-Supported Catalysts Based on a Commercial (BPQ) Zeolite Beta

	Catalyst composition (wt%)				Brönsted acidity[a] ($\mu mol_{pyridine}/g_{zeolite}$)			H_2 consumed[b] (cm^3/mg_{NiMo})
	MoO_3	NiO	Zeolite	γ-Al_2O_3	250°C	350°C	400°C	
NiMo/Al	15	4	0	81	—	—	—	0.38
NiMo/BPQ	15	4	81	0	8	4	1	0.40
NiMo/(BPQ + Al)	15	4	40.5	40.5	5	2	1	0.53
NiMo/Al + BPQ (1:1)	7	2	50	41	24[c]	12[c]	5[c]	0.45
NiMo/Al + BPQ (1:2)	5	1.3	66.6	27	—	—	—	—

[a] Calculated from IR-pyridine and corrected per gram of zeolite in the catalyst.
[b] From TPR.
[c] Calculated considering the Brönsted acidity of the BPQ zeolite (Table 4) and the wt% of zeolite in the hybrid catalyst.

The part concerning the influence of the Si/Al ratio and crystal size of beta zeolite was performed by preparing hybrid catalysts formed by mixing the zeolites with the NiMo/Al (15 wt% MoO_3 and 4 wt% NiO) in a 1:1 ratio by weight.

Finally, for the comparison of the nanocrystalline beta zeolite with conventional supports the NiMo phase (12 wt% MoO_3 and 3 wt% NiO) was directly impregnated onto the different supports.

1.2. Characterization Techniques

Textural properties were determined from the N_2 adsorption isotherms at 77 K on a ASAP-2000 (Micromeritics) apparatus.

The acidity of the supports and NiMo-containing catalysts was measured by infrared spectroscopy with adsorption of pyridine and desorption at different temperatures in a Nicolet 710 FTIR apparatus following the experimental procedure described in (14). Quantitative determination of the amount of Brönsted and Lewis acid sites was derived from the intensities of the IR bands at ca 1450 and 1545 cm^{-1}, respectively and using the extinction coefficients given by Emeis (15).

Transmission electron microscopy (TEM) and scanning electron microscopy (SEM) were carried out in a Philips 400 microscope in order to estimate the crystal size of the beta zeolite samples.

Chemical analyses of the zeolites were obtained by atomic absorption spectrophotometry in a Spectra A-plus (Varian) apparatus.

Temperature programmed reduction (TPR) experiments were performed in a TPD/TPR 2900 equipment (Micromeritics) using a thermal conductivity detector (TCD). For these experiments 20 mg of sample were placed in a quartz cell and heated from ambient temperature up to 950°C at a heating rate of 10°C/min while flowing a mixture of 15 vol% H_2 in He through the sample. The amount of hydrogen consumed was determined using CuO as a reference sample.

1.3. Reaction System and Procedure

Mild hydrocracking of a vacuum gasoil (VGO) feedstock was performed in a fixed bed stainless steel tubular reactor having 2.54 cm ID and 65 cm length. The reactor was loaded with 2.5–7.5 g of catalyst with a particle size of 0.59–0.84 mm diameter, diluted with SiC until a constant bed volume of 12 cm^3. Then, the catalysts were presulfided at atmospheric pressure and 400°C for 3 h using a mixture of 10 vol% H_2S in H_2. The reactions were carried out at 3.0–5.0 MPa total pressure, 375–425°C temperature, and H_2/feed ratio of 1000 Nm^3/m^3. The space velocity, WHSV, was varied between 2 and 6 h^{-1} by changing either the feed rate or the amount of catalyst. Preliminary hydrocracking experiments were carried out to ascertain that under these conditions the reaction was not controlled by external nor intraparticle mass transfer limitations. In all cases the catalytic data reported here correspond to the stationary behavior, which was obtained after a period of operation of ca 6–10 h, depending on the specific catalyst and reaction conditions used. The hydrocracking conversion is defined here as the total yield of products boiling below 360°C, without correcting for the fraction of these products (about 10 wt%) already present in the gasoil feed (Table 2).

The main physicochemical properties of the VGO used are listed in Table 2. The distillation range in the original gasoil and liquid reaction products was determined by simulated distillation (SIMDIS, ASTM D-2887) in a Varian GC 3400 equipped with a FID and a DB-5 column having 5 m length. Analysis of the reaction gases was performed on-line in a Varian GC 3400 equipped with a FID and a capillary column (Petrocol DH-50.2, fused silica, 50 m length). The concentration of sulfur and nitrogen in the liquid products was determined by elemental analysis in a Fisons 1108 CHNS-O instrument.

TABLE 2

Physicochemical Characteristics of the Vacuum Gasoil (VGO) Feed

Sulfur content (wt%)	2.59
Nitrogen content (ppm)	3100
Density, g/cm^3 (60°C)	0.92
Distillation range (°C)	
IBP	123
5	289
10	358
30	417
50	430
70	453
90	485
95	500
FBP	525

2. RESULTS AND DISCUSSION

2.1. Characterization of Catalysts

The chemical composition, average crystallite size, and the textural properties of the different supports and those of the NiMo-catalysts containing 12 wt% MoO_3 and 3 wt% NiO are given in Table 3. All the beta zeolites synthesized presented a pure BEA crystalline phase and a high degree of crystallinity (between 90–100%), as observed by XRD. The sample synthesized in the presence of fluoride (BF9) shows narrower and better resolved XRD peaks as compared to the nanocrystalline beta samples synthesized in basic medium. These features can be related to both the larger crystals and the much lower concentration of structural defects (SiO^-) in the fluoride-made beta sample as compared to the nanocrystalline samples synthesized in basic medium (13). After calcination, a decrease of the crystallinity of about 30–35% with respect to the as-synthesized zeolites is observed for the different beta samples (Table 3), which is in the range typically observed for beta zeolite synthesized in basic or fluoride medium for these Al contents (13).

It is also seen in Table 3 that the approximate crystal size of the nanocrystalline NB8 and NB17 samples is about 10 and 30–50 nm, respectively, as estimated from the TEM photographs. Although these values are only relative, due to the tendency of nanocrystals to agglomerate, they are in good agreement with the values obtained from the external surface area of the as-synthesized samples and calculated assuming a spherical morphology, as reported in (16). On the other hand, the crystal size of the fluoride-made BF9 sample determined from SEM pictures (ca 200 nm) is one order of magnitude larger than that of the nanocrystalline beta samples.

As deduced from the data presented in Table 3, the nanocrystalline NB8 and NB17 samples have a higher mesopore volume (calculated as the difference between the total and micropore volume) than the rest of the beta samples. Such a high mesoporosity is due to the interparticle voids and presents a narrow distribution of pore diameters (16). The nanocrystalline NB17 sample displays a lower mesoporosity than that of sample NB8, but still higher than that of the fluoride-made BF9 sample. All the beta zeolites, except sample NB8, present a micropore volume of about

TABLE 3

Physicochemical Properties of the Different Supports and NiMo-Containing Catalysts (3 wt% NiO and 12 wt% MoO_3)

Sample	Bulk Si/Al atomic ratio	XRD Crystallinity (%)	Crystal size (nm)	BET (m^2/g)	Pore volume (cm^3/g)	
					Total	Micropore[a]
NB8	8	65	10	737	0.96	0.15
NB17	17	70	30-50	568	0.65	0.19
BF9	9	70	200	619	0.45	0.20
BPQ	12	70	150	560	0.49	0.19
USY[c]	28	50	400–600[b]	551	0.41	0.18
SiAl[d]	2.55	—	—	268	0.31	<0.01
Al_2O_3	—	—	—	122	0.21	<0.01
NiMo/NB8	—	40	—	428	0.57	0.09
NiMo/BPQ	—	50	—	341	0.59	0.11
NiMo/USY	—	30	—	283	0.29	0.09
NiMo/SiAl	—	—	—	171	0.29	<0.01
NiMo/Al	—	—	—	104	0.16	<0.01

[a] Obtained by the *t*-plot method.
[b] According to the specifications given by PQ Corp.
[c] $a_0 = 2.425$ nm (framework Si/Al ratio of 99).
[d] SiO_2-Al_2O_3.

0.19–0.20 cm^3/g, which is close to the typical values obtained for beta zeolite by using the *t*-plot method (13). The lower micropore volume of the nanocrystalline NB8 zeolite with lower Si/Al ratio (0.15 cm^3/g) is probably due to the small crystal size, as previously reported (16).

After impregnation with Ni and Mo a reduction of crystallinity and micropore volume is observed for both beta and USY zeolites (Table 3). Many authors have reported a significant loss of crystallinity in NaY and HY zeolites after impregnation of Mo and subsequent calcination at temperatures above 350–400°C, which has been typically associated to a partial destruction of the zeolite structure (17–21). Nevertheless, migration of the oxides into the zeolite channels may produce a partial blockage of the zeolite pores and might also contribute to the observed decrease of micropore volume in the NiMo-containing catalysts.

The acidity of the calcined zeolites, the amorphous silica-alumina, and some of the NiMo-containing catalysts are presented in Table 4. It can be seen that the nanocrystalline NB8 sample has a lower amount of Brönsted acid sites retaining pyridine at 250°C than the BF9 sample prepared in fluoride medium and having similar bulk Si/Al ratio. The differences cannot be explained by considering only the crystallinity of the samples, but one has to assume that a higher amount of Al was extracted from the zeolite lattice on the nanocrystalline as compared to the fluoride-made BF9 sample. The two nanocrystalline samples having different Si/Al ratios show a similar Brönsted acidity at 250°C desorption temperature, suggesting that a higher dealumination took place on sample NB8 with the lowest Si/Al ratio. Accordingly, this presents a higher amount of Lewis acid sites, which are usually related to the presence of highly dispersed extraframework aluminum (EFAL) species formed during the thermal treatments (22). Moreover, all the beta zeolites have a higher amount of Brönsted sites than the USY zeolite, due to the much lower Al content of the latter sample (Table 3). It is also seen in Table 4 that the acidity of the amorphous silica-alumina, both in terms of number and strength of the acid sites, is much lower than that of zeolites.

TABLE 4

Acidity (μmol of Pyridine/g of Solid) of the Supports and NiMo-Containing Catalysts (12 wt% MoO_3 and 3 wt% NiO) as Determined by IR Spectroscopy with Adsorption–Desorption of Pyridine

	Brönsted			Lewis		
Sample	250°C	350°C	400°C	250°C	350°C	400°C
NB8	58	20	15	59	46	40
NB17	59	43	n.d.[a]	47	41	n.d.
BF9	91	50	38	41	40	35
BPQ	49	24	10	72	67	50
USY	20	8	2	12	8	5
SiAl	5	1	-	22	13	-
NiMo/NB8	27	7	4	67	40	27
NiMo/BPQ	20	9	4	42	26	21
NiMo/USY	8	5	2	16	8	3
NiMo/SiAl	1	<0.1	-	4	0.3	-

[a] n.d. = not determined.

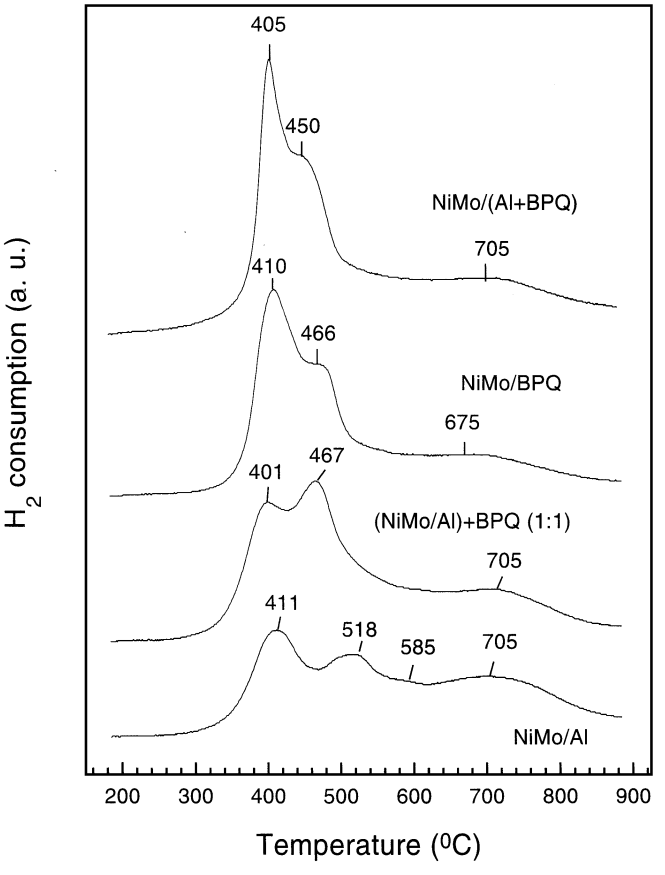

FIG. 1. TPR profiles of NiMo-beta zeolite composites.

After impregnation of metals the amount of Brönsted acid sites decreases with respect to the metal-free supports, and this effect can be ascribed to the interaction of the surface OH groups with the metal precursors (17).

We have studied the reducibility of the metal oxides as a function of their location in the final NiMo-containing catalysts, and the TPR results are presented in Fig. 1. In general, the TPR profiles of the NiMo-zeolite catalysts show three different reduction zones: (a) $400 < T_{max} < 410$°C; (b) $450 < T_{max} < 470$°C, and (c) $T_{max} > 500$°C; the latter corresponds to very refractory Mo species which are strongly interacting with the support. The species reducing in the lowest temperature range have been related to polymolybdate-like phases in the case of NiMo/alumina (23) and NiMo/carbon catalysts (24). It is worth noting that the reducibility of the metal phases present in the hybrid (NiMo/Al) + BPQ catalyst prepared by the mechanical mixture of NiMo/γ-Al_2O_3 and the commercial beta zeolite is higher than those formed in the NiMo/γ-Al_2O_3

component alone. We have not, at present, an interpretation for this result. Figure 1 also shows that the reducibility of the metal oxides in the beta zeolite-containing catalyst is similar, although the relative proportion of species reducing in the low (400–410°C) and medium (450–470°C) ranges varies, depending on the specific location of the metals during the preparation of catalysts. Thus, it appears that the proportion of species reducing at lower temperatures increases when the metals are totally or partially impregnated onto the zeolite (samples NiMo/BPQ and NiMo/(Al + BPQ), respectively) with respect to the hybrid (NiMo/Al) + BPQ catalyst, where the metals are located exclusively on the alumina component. The amount of hydrogen consumed during the TPR experiments has been included in Table 1. It is seen there that the consumption of H_2 is lower for the NiMo/Al sample, as compared to the zeolite-containing catalysts. This suggests a lower degree of reduction of the oxidic species, probably due to a higher dispersion of the metals on the alumina surface. It is also seen that the consumption of hydrogen is higher for the hybrid (NiMo/Al) + BPQ sample as compared to the NiMo/Al component alone, in agreement with the increased reducibility of the metals on the alumina in the presence of the zeolite, as observed from the TPR profiles. On the other hand, the highest consumption of hydrogen occurs when the NiMo phase is impregnated totally or partially on the beta zeolite.

2.2. Mild Hydrocracking of Vacuum Gasoil

Influence of the Location of Metals in the NiMo-Beta Zeolite Catalysts

Typical hydrocracking catalysts based on metal sulfides combine the hydrogenation–dehydrogenation function of the sulfides with the acidity of the zeolite support. In order to obtain a pure bifunctional behavior, a good balance between the hydrogenation and acidic sites has to be achieved, the latter being mainly responsible for the cracking reactions (25). Moreover, in order to avoid undesirable secondary reactions that lead to a fast deactivation of the acid sites, a rapid diffusion of the intermediate species between both kinds of sites has to be achieved. This will be determined by the distance between the hydrogenation and acidic sites, which will depend on the location of the metals during the preparation of the catalyst. In this part of the work we have studied the influence of this variable by preparing a series of zeolite-based NiMo catalysts, in where the metal precursors have been directly impregnated onto the zeolite component (sample NiMo/BPQ), on a physical mixture of the beta zeolite and γ-Al_2O_3 in a ratio of 1 : 1 wt/wt (sample NiMo/(Al + BPQ)), or on separate particles by mechanically mixing the NiMo/γ-Al_2O_3 component and the beta zeolite (sample (NiMo/Al) + BPQ). In this latter case two catalysts with a (NiMo/Al)/BPQ ratio of 1 : 1 and 1 : 2 by weight were prepared (see the composition of the catalysts in Table 1). Here it has to be considered that, due to the relatively low surface area of the γ-Al_2O_3 used (Table 3), the metal sulfides are probably not strongly anchored to the alumina surface, and then a migration of the sulfides from this component to the zeolite cannot be discarded. After *in-situ* sulfidation the activity of the catalysts was evaluated for the hydroconversion of VGO at 375°C, 5.0 MPa and using a H_2/feed ratio of 1000 Nm^3/m^3. The space velocity, WHSV, used in these experiments was adjusted to keep constant the total amount of metal sulfides in the catalyst bed.

Figure 2a shows the activity of the catalysts for the hydrocracking (HCK), hydrodesulfurization (HDS), and hydrodenitrogenation (HDN) reactions under the given reaction conditions. As observed, the hybrid (NiMo/Al) + BPQ

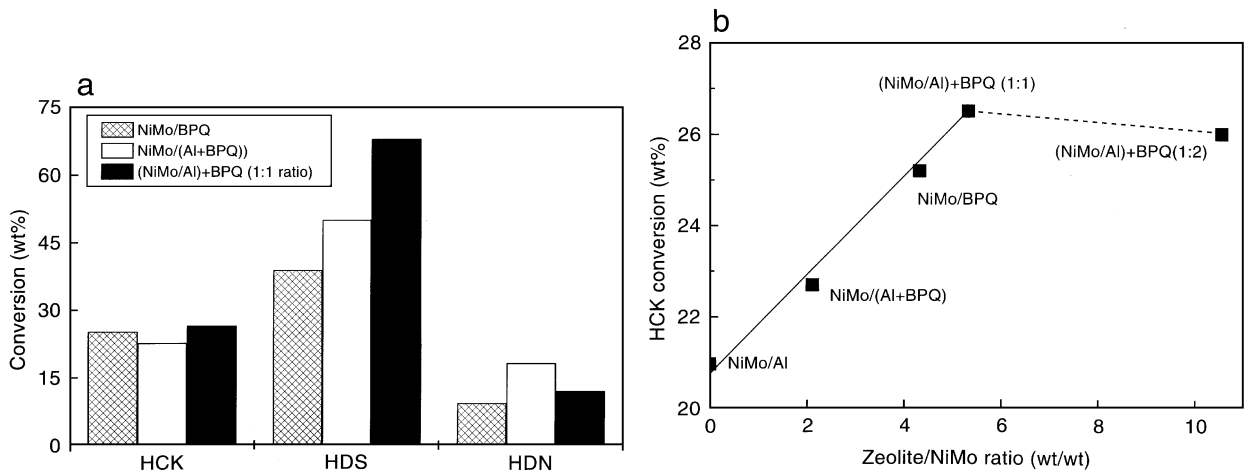

FIG. 2. (a) Influence of the location of NiMo during the preparation of beta-based catalysts on the hydrocracking (HCK), hydrodesulfurization (HDN), and hydrodenitrogenation (HDN) activities obtained at 375°C, 5.0 MPa, and H_2/feed ratio of 1000 Nm^3/m^3; (b) HCK conversion as a function of the zeolite/NiMo ratio.

sample (1 : 1 ratio) gives a slightly higher hydrocracking conversion than the NiMo/BPQ sample, and this is more active than the NiMo/(Al + BPQ) catalyst. This trend of activity correlates well with the zeolite/NiMo ratio in the catalyst (Fig. 2b). However, it has to be considered that the acidity of the catalysts may change depending on the location of the NiMo phase. In fact, the acidity data given in Table 1 show that the amount of Brönsted acid sites in the calcined solids is lower when the NiMo is impregnated on a mixture of zeolite and γ-Al_2O_3 than on the beta zeolite directly (NiMo/BPQ), and this is lower than for the hybrid catalyst formed by a physical mixture of NiMo/Al and the zeolite (1 : 1 ratio). This trend of acidity also correlates, qualitatively, with the observed hydrocracking activity. It is worth noting from Fig. 2b that the NiMo/Al catalyst already presents some activity for hydrocracking. According to the bifunctional catalysis, Brönsted acid sites are supposed to be responsible for the cracking reactions by protonating the olefin formed after dehydrogenation of the alkanes on the metallic sites (26, 27). Some authors have reported the presence of Brönsted acidity in sulfide (Co)Mo/Al_2O_3 (28, 29) and in oxide NiMo/Al_2O_3 (30), and this might explain the activity of the NiMo/Al catalyst for hydrocracking (Fig. 2b).

The fact that the hydrocracking conversion is higher for the hybrid catalyst, where the metal sulfides are present in separate NiMo/Al_2O_3 particles, suggests that the distance between the hydrogenation and acidic sites is low enough to prevent a severe deactivation of the Brönsted acid sites of the beta zeolite by coking. This can be explained by considering that hydrogen *spillover* from the NiMo sulfides located on the alumina component to the acid sites in the zeolite occurs (31, 32). This will supply activated hydrogen necessary to hydrogenate and desorb the olefinic intermediates from the zeolite acid sites that otherwise would lead to extensive coking and catalyst deactivation (33). In fact, when the amount of zeolite in the hybrid catalyst is increased to a proportion of (NiMo/Al) : BPQ of 1 : 2 by weight, no further increase of the HCK conversion was observed (Fig. 2b). If the reaction rate is limited by the migration of the olefin intermediates from the metal centers to the acid sites, then an insufficient dehydrogenation activity in the hybrid catalyst with a higher proportion of zeolite (NiMo/Al-to-zeolite ratio of 1 : 2) may explain the low hydrocracking activity of this sample.

On the other hand, the activity towards HDS is observed to be highest for the hybrid (NiMo/Al) + BPQ catalyst (Fig. 2a). Indeed, the HDS obtained with this catalyst is very similar to that obtained on the NiMo/alumina component alone (not shown). This indicates that the NiMo sulfide phases present on the alumina surface have a higher efficiency for sulfur removal than those located directly on the zeolite surface, probably due to a better dispersion of the sulfides in the former catalyst. Similar results have been reported during the hydrocracking of VGO on NiMo/HY catalysts (34). Accordingly, the NiMo/(Al + BPQ) catalyst, where the sulfides are present on both the alumina and zeolitic components, displays a HDS activity intermediate between the other two samples.

TABLE 5

Influence of the Location of the Metal Sulfides on the Selectivity to the Different Hydrocracked Fractions Obtained at about 50–60% Hydrocracking Conversion

Catalyst	Selectivity (wt%)		
	Gases[a]	Naphtha[b]	Middle distillates[c]
MiMo/BPQ	19.5	29.2	51.3
NiMo/(BPQ + Al)	18.0	23.9	58.1
NiMo/Al + BPQ (1 : 1)	19.3	24.8	55.9
NiMo/Al + BPQ (2 : 1)	18.0	25.4	56.6

[a] Gases: C_1–C_4.
[b] Naphtha: C_5—195°C bp.
[c] Middle distillates: 195–360°C bp.

A different situation occurs for the HDN reaction. As observed in Fig. 2a, the HDN conversion is highest when the metals are incorporated on a mechanical mixture of the beta zeolite and γ-alumina (sample NiMo/(Al + BPQ)). These results suggest that the HDN activity is enhanced by a close cooperation between the hydrogenating sites associated with the metal sulfides and the Brönsted acidity of the zeolitic component. The importance of the dual functionality for the HCK and HDN reactions of zeolite-based hydrocracking catalysts has also been observed in the case of NiMo-HY samples (34).

The selectivity to the different hydrocracked fractions obtained at ca 50–60% HCK conversion is compared in Table 5. As observed, the NiMo/BPQ sample gives the highest selectivity to gases and naphtha, whereas a better selectivity towards the desired middle distillate fraction is observed for the catalyst where the metals were impregnated on a physical mixture of alumina and Beta zeolite, NiMo/(Al + BPQ). This may be explained considering the lower metal dispersions achieved when the oxide precursors are impregnated directly on the zeolite, as deduced from the TPR results given in Fig. 1. This would produce a unbalance between the acidic and hydrogenation functions in favor of the former, which results in a higher gasoil cracking activity producing more gases and naphtha in the NiMo/BPQ catalyst. In the case of the hybrid (NiMo/Al) + BPQ catalyst (1 : 1 ratio) and owing to the better dispersion of the metals on the alumina component, hydrogen dissociated on the metals is spilt-over to the zeolite, making the catalyst behave as a true bifunctional catalyst.

Influence of the Si/Al Ratio and Crystal Size of Beta Zeolite

In this section we address the influence of the Si/Al ratio of the nanocrystalline beta zeolite and the influence of

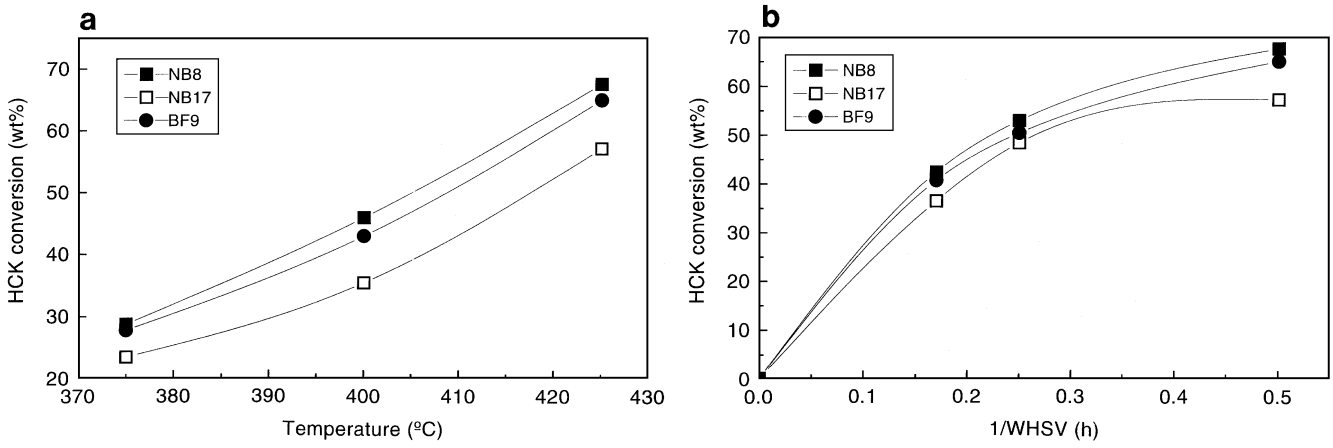

FIG. 3. Hydrocracking conversion obtained for the composite (NiMo/Al) + zeolite catalysts prepared from nanocrystalline beta samples with different Si/Al ratio (NB8 and NB17) and from the fluoride-made beta zeolite with larger crystals (BF9): (a) as a function of reaction temperature at constant space velocity (WHSV = 2 h^{-1}), and (b) as a function of contact time (1/WHSV) at constant temperature (425°C).

the zeolite crystal size by comparing the results obtained with the nanocrystalline samples and with a beta zeolite prepared in fluoride medium. This study has been done by preparing hybrid catalysts on which the hydrogenation function is given in separate NiMo/γ-Al_2O_3 particles, which are then admixed with the acidic zeolite in a proportion of 50/50 by weight. The amount of metals impregnated on the alumina was 15 wt% MoO_3 and 4 wt% NiO, and therefore, the composition of the final catalysts is the same as that given in Table 1 for the (NiMo/Al) + BPQ catalyst (1 : 1).

The hydrocracking conversion obtained at a constant space velocity (WHSV = 2 h^{-1}) over the hybrid catalysts is shown in Fig. 3a as a function of reaction temperature. As observed, the conversion increases when decreasing the Si/Al ratio of the nanocrystalline beta samples, that is, when increasing the aluminum content. The fact that both samples showed similar Brönsted acidity at 250°C pyridine desorption (Table 4) suggests that the better catalytic performance of the nanocrystalline beta sample with lowest Si/Al ratio is probably related to its higher mesoporosity and external surface area. Moreover, when compared at similar Si/Al ratio, the catalyst containing the nanocrystalline beta zeolite (NB8) is slightly more active than that prepared from the sample synthesized in fluoride medium and having larger crystals (BF9), despite the latter zeolite having a larger amount of Brönsted acid sites as determined by pyridine adsorption (Table 4). As above, this result can be ascribed to the higher mesoporosity of the nanocrystalline sample, which determines a greater amount of external acid sites which are available to the large molecules encountered in the gasoil feed. The same trend between the three samples is observed when the hydrocracking conversion is varied by changing the space velocity at constant reaction temperature (425°C), as shown in Fig. 3b.

The yields to the different hydrocracked fractions obtained at 425°C is plotted versus the HCK conversion in Figs. 4a–c. As observed there, the catalysts based on the nanocrystalline samples produce fewer gases and more middle distillates than the catalyst prepared from the beta sample with larger crystals. Furthermore, the product distribution is very similar for the two nanocrystalline samples having different Si/Al ratios. These results indicate that diffusion of the molecules formed in the primary cracking events (middle distillate) is strongly favored in the very small crystallites of the NB8 and NB17 zeolites, whereas secondary cracking of these molecules leading to smaller fragments (gases) is more favored on the beta zeolite with larger crystallites, BF9.

In these experiments we also determined the extent of HDS and HDN reactions at different levels of hydrocracking conversion, and the results obtained are presented in Figs. 5 and 6, respectively. The results in Fig. 5 show that the two catalysts based on the nanocrystalline beta samples are more active towards hydrodesulfurization (HDS) than that based on the fluoride-made zeolite and that for the nanocrystalline samples the HDS activity increases when increasing the Si/Al ratio. However, the hydrodenitrogenation (HDN) activity (Fig. 6) is higher for the samples with lower Si/Al ratio, this case also having higher activity for the nanocrystalline beta sample.

The above results clearly illustrate the benefits of using small zeolite crystallites on the activity of zeolite-based NiMo catalysts towards the HCK, HDS, and HDN reactions. This beneficial effect can be related with a higher amount of Brönsted acid sites accessible to the large molecules in the gasoil feed, and probably also with a synergism between the surface acid sites on the zeolite and the metal sulfides on the alumina component, leading to higher HDS and HDN activities and lower coking tendency in the

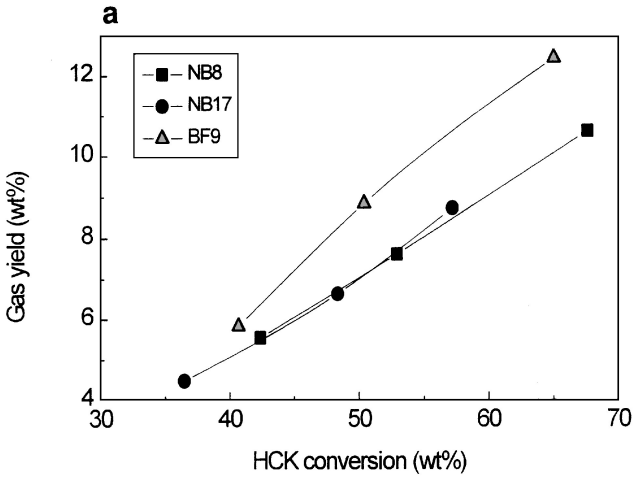

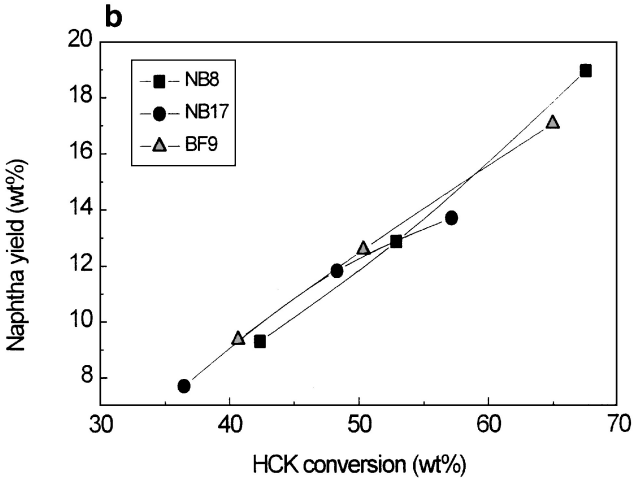

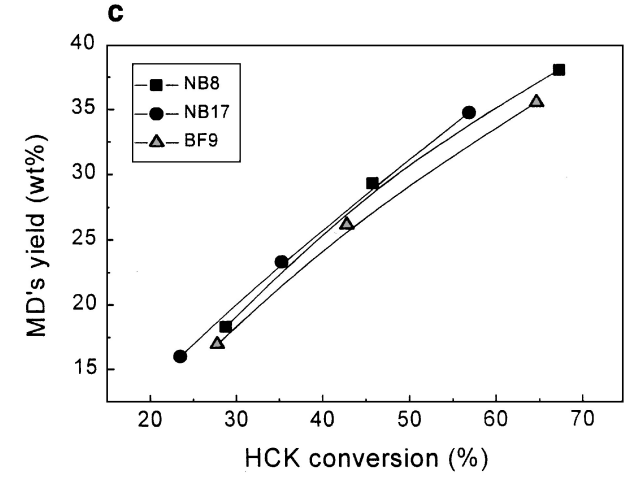

FIG. 4. Yield to gases (a), naphtha (b), and middle distillates (c) at different hydrocracking conversions obtained for the nanocrystalline and fluoride-made beta-based catalysts. The hydrocracking conversion has been changed by varying the WHSV at constant reaction temperature (425°C). Reaction conditions: $P = 3.0$ MPa, H_2/feed ratio of 1000 Nm^3/m^3.

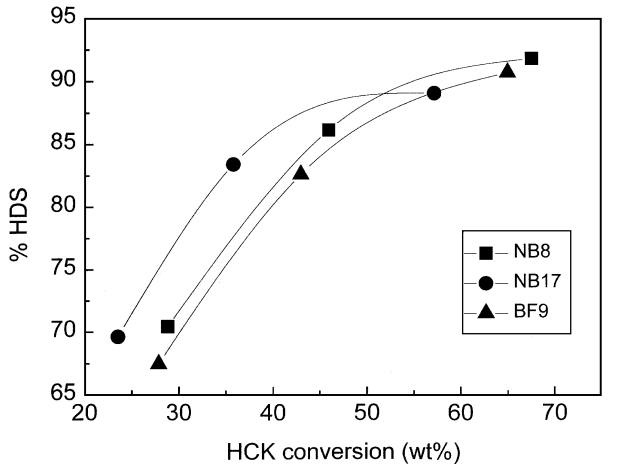

FIG. 5. Hydrodesulfurization (HDS) conversion obtained at different hydrocracking levels for the composite NiMo-zeolite catalysts prepared from nanocrystalline and fluoride-made beta samples. The hydrocracking conversion has been varied by changing the reaction temperature at constant WHSV (2 h^{-1}). Reaction conditions: $P = 3.0$ MPa, H_2/feed ratio of 1000 Nm^3/m^3.

case of the nanocrystalline beta catalysts. Furthermore, the use of very small crystallites results in a higher selectivity to the desired middle distillates, as a consequence of the faster diffusion of the intermediate products and lower recracking rates.

Comparison of Nanocrystalline Beta with Conventional Supports

In this part of the work we compare the catalytic performance of the nanocrystalline beta zeolite (sample NB8, Si/Al = 8) with other materials that are commonly used as

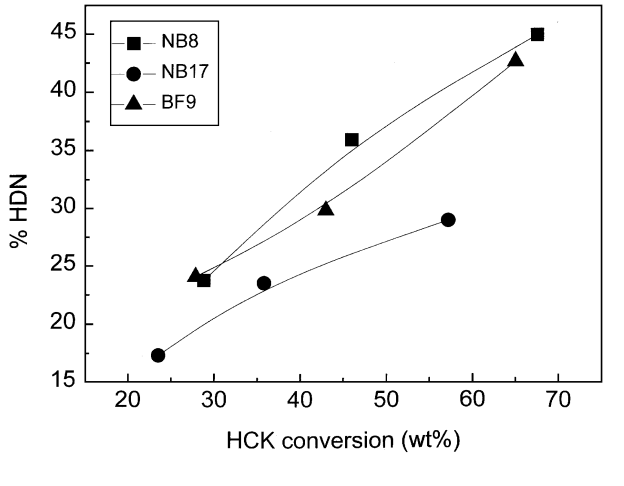

FIG. 6. Hydrodenitrogenation (HDN) conversion obtained at different hydrocracking levels for the composite NiMo-zeolite catalysts prepared from nanocrystalline and fluoride-made Beta samples. Reaction conditions as in Fig. 5.

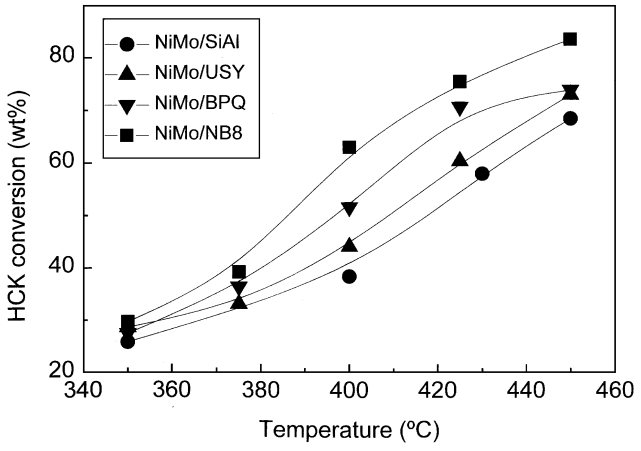

FIG. 7. Hydrocracking (HCK) activity of different NiMo-supported catalysts as a function of reaction temperature. Reaction conditions: $P =$ 3.0 MPa, WHSV $= 2\ h^{-1}$, H_2/feed ratio of 1000 Nm^3/m^3.

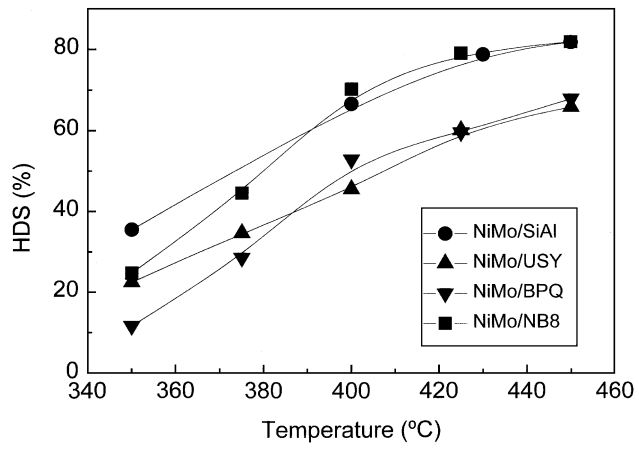

FIG. 8. Hydrodesulfurization (HDS) activity of NiMo-supported catalysts as a function of reaction temperature. Reaction conditions as in Fig. 7.

supports in the formulation of hydrocracking catalysts, such as amorphous silica-alumina (SiAl) and an ultrastable low unit cell size Y zeolite (USY). Moreover, the results obtained on a commercial beta sample (BPQ) are also included in the comparison. For this study the NiMo precursors were directly impregnated on the acidic supports in a concentration of 12 wt% MoO_3 and 3 wt% NiO.

Concerning the hydrocracking activity, the results in Fig. 7 show that the catalysts based on beta are more active than the one based on USY zeolite, with the amorphous silica-alumina being less active for hydrocracking. Among the two beta samples, the nanocrystalline NB8 zeolite gives a higher hydrocracking conversion. The order of activity for hydrocracking corresponds well with the Brönsted acidity of the NiMo-supported catalysts before sulfidation as determined by pyridine adsorption (Table 4).

Furthermore, the selectivities to the different hydrocracking fractions calculated at ca 50% hydrocracking conversion are given in Table 6. As observed, the nanocrystalline beta zeolite gives the lowest selectivity to gases, indicating a low recracking activity. Consequently, the selectivity towards middle distillates is high in the NiMo/NB8 catalyst, which is even more selective to these products than the catalyst based on amorphous silica-alumina which is the preferred support for maximizing the yield to middle distillates in commercial hydrocracking catalysts (3).

On the other hand, the catalyst based on the nanocrystalline beta zeolite displays an HDS activity similar to that obtained on the amorphous silica-alumina catalyst, and much higher at a given reaction temperature than the activity of the catalysts based on the commercial beta and USY zeolites (Fig. 8). The higher external surface area of the nanocrystalline beta (ca 400 m^2/g, estimated from N_2 adsorption), as compared to the commercial beta (ca 180 m^2/g) and USY (ca 190 m^2/g) would favor a better dispersion of the active phase for the HDS reaction. Consequently, the behavior of the NiMo/NB8 catalyst resembles more that of the high surface area (268 m^2/g) amorphous silica-alumina with respect to the HDS activity.

TABLE 6

Selectivity to the Hydrocracked Fractions Obtained at ca 50% Hydrocracking Conversion on the Different NiMo-Supported Catalysts Containing 12 wt% MoO_3 and 3 wt% NiO

	Selectivity (wt%)		
Catalyst	Gases[a]	Naphtha[b]	Middle distillates[c]
NiMo/NB8	11.4	32.7	55.9
NiMo/BPQ	15.0	34.5	50.5
NiMo/USY	17.1	33.3	49.6
NiMo/SiAl	15.8	29.6	54.6

[a] Gases: C_1–C_4.
[b] Naphtha: C_5—195°C bp.
[c] Middle distillates: 195–360°C bp.

3. CONCLUSIONS

Beta zeolite shows good performance for mild hydrocracking of vacuum gasoil. When composite NiMo-γ-Al_2O_3-beta catalysts are prepared it has been shown that better results are obtained when the NiMo are not on the beta zeolite but on the alumina component of the catalyst. An intermediate behavior was observed when the metals are supported on a physical mixture of both components, i.e. γ-Al_2O_3 and beta. The crystallite size of the zeolite plays an important role, and the smaller the crystallites of the beta zeolite the better is the catalytic activity towards hydrocracking and HDS reactions, and the higher is the selectivity towards the desired middle distillate fraction. It

has been shown also that the catalyst based on nanocrystalline beta gives better results than those based on USY zeolite and amorphous silica-alumina.

ACKNOWLEDGMENT

Financial support by the Comisión Interministerial de Ciencia y Tecnología (CICYT) of Spain (Project MAT97-1010) is gratefully acknowledged.

REFERENCES

1. Ward, J. W., *Fuel Process. Technol.* **35**, 55 (1993).
2. Bridge, A. G., Cash, D. R., and Mayer, J. F., "NPRA Annual Meeting, San Antonio, TX, March 1993," AM-93-60.
3. Scherzer, J., and Gruia, A. J., *in* "Hydrocracking Science and Technology," Chap. 12, p. 215. Dekker, New York, 1996.
4. Trambouze, P., *in* "Chemical Reactor Technology for Environmentally Safe Reactors and Products" (H. I. de Lasa *et al.*, Eds.), p. 425. Kluwer Academic, Amsterdam, 1993.
5. Dufresne, P., Bigeard, P. H., and Billon, A., *Catal. Today* **1**, 367 (1987).
6. Stanislaus, A., and Cooper, B. H., *Catal. Rev. Sci. Eng.* **36**, 75 (1994).
7. Corma, A., Martínez, A., and Martínez-Soria, V., *J. Catal.* **153**, 25 (1995).
8. Rajagopalan, K., Peters, A. W., and Edwards, G. C., *Appl. Catal.* **23**, 69 (1986).
9. Camblor, M. A., Corma, A., Martínez, A., Mocholí, F. A., and Pérez-Pariente, J., *Appl. Catal.* **55**, 65 (1989).
10. Ward, J. W., U.S. Patent 5,279,726 (1994).
11. Occelli, M. L., U.S. Patent 5,374,349 (1994).
12. Camblor, M. A., Corma, A., Mifsud, A., Pérez-Pariente, J., and Valencia, S., *Stud. Surf. and Catal.* **105**, 341 (1997).
13. Camblor, M. A., Corma, A., and Valencia, S., *J. Mater. Chem.*, in press.
14. Corma, A., Fornés, V., Martínez, A., and Orchillés, A. V., *ACS Symp. Ser.* **368**, 542 (1988).
15. Emeis, C. A., *J. Catal.* **141**, 347 (1993).
16. Camblor, M. A., Corma, A., and Valencia, S., *Microp. and Mesop. Mater.*, in press.
17. Corma, A., Vazquez, M. I., Bianconi, A., Clozza, A., García, J., Pallota, O., and Cruz, J. M., *Zeolites* **8**, 464 (1988).
18. Lopez Agudo, A., Cid, R., Orellana, F., and Fierro, J. L. G., *Polyhedron* **5**, 187 (1986).
19. Cid, R., Orellana, F., and Lopez Agudo, A., *Appl. Catal.* **32**, 327 (1987).
20. Thoret, J., Marchal, C., Doremieux-Morin, C., Man, P. P., Gruia, M., and Fraisard, J., *Zeolites* **13**, 269 (1993).
21. Okamoto, Y., *Catal. Today* **39**, 45 (1997).
22. Corma, A., Fornés, V., Martínez, A., and Sanz, J., *ACS Symp. Ser.* **446**, 17 (1988).
23. Brito, J. L., and Laine, J., *J. Catal.* **139**, 540 (1993).
24. Matos, J., Brito, J. L., and Laine, J., *Appl. Catal A: General* **152**, 27 (1997).
25. Weikamp, J., and Ernst, S., *in* "Guidlines for Mastering the Properties of Molecular Sieves" (D. Barthomeuf *et al.*, Eds.), p. 343. Plenum, New York, 1990.
26. Martens, J. A., Jacobs, P. A., and Weitkamp, J., *Appl. Catal.* **20**, 239 (1986).
27. Martens, J. A., Tielen, M., and Jacobs, P. A., *Catal. Today* **1**, 435 (1987).
28. Topsøe, N.-Y., Topsøe, H., and Massoth, F. E., *J. Catal.* **119**, 252 (1989).
29. Topsøe, N.-Y., and Topsøe, H., *J. Catal.* **139**, 641 (1993).
30. Park, Y.-C., Oh, E.-S., and Rhee, H.-K., *Ind. Eng. Chem. Res.* **36**, 5083 (1997).
31. Stumbo, A. M., Grange, P., and Delmon, B., *Stud. Surf. Sci. and Catal.* **106**, 225 (1997).
32. Rodriguez, N. M., and Baker, R. T. K., *J. Catal.* **140**, 287 (1993).
33. Roessner, F., and Roland, U., *J. Mol. Catal. A: Chemical* **112**, 401 (1996).
34. Shimada, H., Yoshitomi, S., Sato, T., Matsubayashi, N., Imamura, M., Yoshimura, Y., and Nishijima, A., *Stud. Surf. and Catal.* **106**, 115 (1997).